2. Steiner, R. E. and Radda, G. K. (eds.), *Nuclear Magnetic Resonance and its Clinical Applications*, Churchill Livingstone, London, 1984.
3. Gupta, R. K. (ed.), *NMR Spectroscopy of Cells and Organisms*, CRC Press, Boca Raton, 1987.
4. Cohen, S. M. (ed.), *Anals of the New York Academy of Sciences*, 'Physiological NMR Spectroscopy: From Isolated Cells to Man', The New York Academy of Sciences, New York, 1987.
5. Sarkar, S. K., Holland, G. A., Lenkinski, R. E., Mattingly, M. and Kinter, L. B., *Magn. Reson. Med.*, 1988, **7**, 117.
6. Sarkar, S. K., Rycyna, R. E., Lenkinski, R. E., Solleveld, H. A. and Kinter, L. B., *Magn. Reson. Med.*, 1991, **17**, 328.
7. Barone, F. C., Clark, R. K., Feuerstein, G., Lenkinski, R. E. and Sarkar, S. K., *Brain Res. Bull.*, 1991, **26**, 285.
8. Sarkar, S. K., Mattingly, M. A., Kline, T. and Greig, R., *Invest. Radiol.*, 1988, **23**, 677.
9. Sarkar, S. K., Clark, R. K., Rycyna, R. E., Mattingly, M. A. and Greig, R., *Magn. Reson. Med.*, 1989, **12**, 268.
10. Morris, P. G., *Nuclear Magnetic Resonance Imaging in Medicine and Biology*, Clarendon Press, Oxford, 1986.
11. Mansfield, P. and Morris, P. G., *NMR Imaging in Biomedicine*, Academic Press, New York, 1982.
12. Edelstein, W. A., Hutchinson, J. M. S. and Johnson, G., *Phys. Med. Biol.*, 1980, **25**, 751.
13. Ernst, R. R. and Anderson, W. A., *Rev. Sci. Instrum.*, 1966, **37**, 93.
14. Haase, A., Frahm, J. and Matthaei, D., *J. Magn. Reson.*, 1986, **67**, 258.
15. Mansfield, P. and Grannel, P. K., *Phys. Rev.*, 1975, **B12**, 3618.
16. Lauterbur, P. C., *IEEE Trans. Nucl. Sci. NS.*, 1984, **31**, 1010.
17. Eccles, C. D. and Callaghan, P. T., *J. Magn. Reson.*, 1986, **68**, 393.
18. Callaghan, P. T. and Eccles, C. D., *J. Magn. Reson.*, 1987, **71**, 426.
19. Callaghan, P. T. and Eccles, C. D., *J. Magn. Reson.*, 1988, **78**, 1.
20. Cho, Z. H., Ahn, C. B. and Juh, S. C., *Med. Phys.*, 1989, **15**, 815.
21. Hoult, D. I. and Richards, R. E., *J. Magn. Reson.*, 1976, **24**, 71.
22. Kundel, H. L., Schlakman, B., Joseph, P. M., Fishman, J. E. and Summer, S. R., *Invest. Radiol.*, 1986, **21**, 12.
23. Wolf, G. L. and Fobben, E. S., *Invest. Radiol.*, 1984, **19**, 324.
24. Kinter, L. B., Shier, W., Flamenbaum, W. and Beeuwkes, R., *Renal Physiol.*, 1982, **5**, 278.
25. Weiner, I. M. and Mudge, G. H., in *The Pharmacological Basis of Therapeutics* (eds. Gilman, A. G., Goodman, L. S., Rall, Murad, T. W.), MacMillan, New York, 1985.
26. James, A. E., Hosain, F., DeLand, F. H., Reba, R. C., Wagner, H. N. and North, W. A., *J. Can. Assoc. Radiol.*, 1971, **22**, 136.
27. Klopper, J. F., Hauser, W., Atkins, H. L., Eckelman, W. C. and Richards, P., *J. Nucl. Med.*, 1972, **13**, 107.
28. Reba, R. C., Hosain, F. and Wagner, H. N., *Radiology*, 1968, **90**, 117.
29. Bradley, R. H., Kent, T. A., Eisenberg, H. M., Quast, M. J. and Ward, G. A., *Stroke*, 1989, **20**, 1032.
30. Brant–Zawadzki, M., Weinstein, P., Bartowski, H. and Moseley, M., *AJR*, 1987, **148**, 579.
31. Sauter, A. and Rudin, M., *Stroke*, 1986, **17**, 1228.
32. Beall, P. T., Amtey, S. and Kasturi, S. R., *NMR Data Handbook for Biomedical Applications*, Pergamon Press, New York, 1984.
33. Clark, R. K., Turner, N. A., Sarkar, S. K. and Greig, R., Abstract of the International Symposium on Critical Determinants in Cancer Progression and Metastasis, Houston, TX, 1989.
34. Sarkar, S. K. and Macartney, L. N., Unpublished results.
35. Caputo, G. R., Sechtem, U., Tscholakoff, D., Higgins, C. B., *AJR*, 1987, **149**, 237.
36. Borah, B. and Szevereny, N. M., *Magn. Reson. Med.*, 1990, **15**, 246.
37. Johnson, G. A. and Maronpot, R. R., *Toxicol. Pathol.*, 1989, **17**, 613.
38. Johnson, G. A., Thompson, M. B., Gewalt, S. L. and Hayes, C. E., *J. Magn. Reson.*, 1986, **68**, 129.
39. McFarland, E., Koutcher, J. A., Rosen, B. R., Teicher, B. and Brady T. J., *J. Comput. Ass. Tomog.*, 1985, **9**, 8.
40. Ra, J. B., Hilal, S. K. and Cho, Z. H., *Magn. Reson. Med.*, 1986, **3**, 296.

ACKNOWLEDGEMENT. We thank our collaborators, Drs. Frank Barone, Robert Clark, Rasesh Kapadia, Lewis Kinter, Robert Lenkinski, Mark Mattingly and Robert Rycyna.

Image-guided *in vivo* proton magnetic resonance spectroscopy in human brain

Ponnada A. Narayana and Edward F. Jackson

The University of Texas Health Science Center at Houston, Department of Radiology, 6431 Fannin, MSMB 2.132, Houston, Texas 77030, USA

Image-guided *in vivo* proton magnetic resonance spectroscopy (MRS) studies of human brain are described. The technical requirements for performing these studies are briefly reviewed. *In vivo* proton MRS brain studies of normal volunteers, patients with multiple sclerosis, and ischaemic brain injury are presented.

THE introduction of powerful Fourier-transform (FT) techniques and continuously decreasing costs and expanding power of computers have propelled nuclear magnetic resonance (NMR) into diverse disciplines. In the last two decades NMR has also been added to the armamentation of diagnostic tools employed in clinics. Because of the connotation the word 'nuclear' carries to a lay person, NMR is simply referred to as magnetic resonance or MR by clinicians and scientists involved in human research. Unfortunately, this nomenclature is a misnomer because magnetic resonance includes not only nuclear magnetic resonance but also electron paramagnetic resonance. Nevertheless, to be consistent with the biomedical literature, we use MR instead of NMR in this review.

Magnetic resonance has a unique role in the medical field because of its ability to provide excellent anatomical details and tissue biochemical information. The anatomical information is obtained through magnetic resonance imaging (MRI) while magnetic resonance spectroscopy (MRS) provides *in vivo* tissue biochemical information. Even though generally the same biochemicals are found in different tissues, the magnetic resonance spectrum is specific to the type of tissue. In addition, the relative amplitudes and chemical shifts of various resonances depend on the tissue state, i.e. the spectrum reflects the tissue health. This quantitative dependence of spectral parameters on the disease state allows the utilization of MRS to monitor the disease objectively and noninvasively.

For a number of reasons MRI and MRS have evolved more or less independently. In order to generate MRI images, MR data are usually acquired in the presence of a gradient referred to as the 'read gradient' for encoding frequency into spatial coordinates. This 'read gradient' destroys the chemical shift information which is the heart and soul of spectroscopy. On the other hand, spectroscopy on its own provides little information about the spatial origin of the spectrum. Thus for *in vivo* MRS to be useful, it is essential to integrate MRI and MRS. Such an integration provides an unprecedented opportunity to characterize tissue and can be considered as a 'noninvasive biopsy'. Since MRS employs low energy radiation and is noninvasive, it is possible to perform *in vivo* studies repeatedly to follow the effect of therapeutic intervention on the disease. Such an ability to continuously monitor the disease state will enable customizing the patient treatment on an individual basis.

Unlike MRI which generally relies on proton resonance due to abundance of water in tissue, MRS studies can be performed on a number of nuclei which includes ^{1}H, ^{13}C, ^{23}Na and ^{31}P. In this review we concentrate only on ^{1}H MRS for many reasons. Proton is the most MR-sensitive nucleus. It provides access to water and a number of biomolecules, including lipids, various amino acids, lactate, and neurotransmitters such as glutamate and γ-amino-butyric acid. There are, however, two major challenges associated with ^{1}H MRS studies. First, the range of proton chemical shifts is narrow and in order to resolve various resonances it is necessary to have a high degree of magnetic field homogeneity. With the availability of high quality magnets and the ability to perform both global and localized shimming, it is now relatively easy to homogenize the magnetic field over the region-of-interest (ROI). The second problem arises because of dynamic range considerations. The typical concentrations of various biomolecules in tissue are on the order of 5 to 10 mM compared to a water concentration of around 40 M. Thus for detecting the resonances from these metabolites with relatively low concentrations, it is essential to suppress the water resonance without a concomitant decrease in the metabolite signals. With the introduction of a number of innovative techniques, it is now possible to suppress water by a factor greater than 1000. These aspects are discussed in detail below.

It is not our intention to review the field of ^{1}H MRS exhaustively. Rather we describe some of the *in vivo* human MRS studies that are currently performed in the authors' laboratory. Because of our primary interest in ^{1}H MRS, the very important and exciting ^{13}C and ^{31}P MR studies are not included in this review. Also, MRS studies of tumours, an extremely important area of *in vivo* MRS research, is not included. However, many of these areas have recently been reviewed by others[1-5]. In this article we concentrate on brain studies only. The MRS data on brain are particularly valuable because routine biopsy of neural tissue is not a recommended procedure. From a practical consideration, in contrast to organs like heart, liver, etc., the lack of physical motion makes the brain well suited for MRS studies.

This review is divided into two major sections. The first section deals with the technical aspects of MRS, viz. spatial localization based on MR images, water suppression, and pulsed gradient fields. The second section deals with the application of proton MRS to the study of brain both in normals and patients with multiple sclerosis and ischaemic brain injury (stroke).

Techniques

Localization

In vivo MRS is meaningful only if the spectral data originate exclusively from the ROI. Isolating the ROI from the rest of the tissue for the purpose of MRS data acquisition is referred to as localization. An ideal localization scheme should satisfy a number of requirements. First, it should be image-based so that the ROI can be selected on a standard MR image. Second, it should be possible to vary the size and position of the ROI anywhere in the body. Third, the technique should provide localization in a single shot. This requirement has a very practical implication. The ROI is typically much smaller than the whole organ. Since the magnetic field needs to be homogenous only over the ROI and because it is easier to achieve higher uniformity over a smaller volume, it is desirable, and in fact essential, to homogenize the magnetic field over the ROI. The scheme that provides a single-shot localization would allow shimming over the localized region. Finally, for patient comfort and safety the localization scheme should require minimum set-up time and utilize the least amount of radiofrequency (RF) power

possible. Of the many localization schemes proposed and reviewed in the literature[6,7], relatively few techniques satisfy many of the requirements indicated above. Of these few, the stimulated-echo (STE) sequence[8–11] has gained wide popularity for ^{1}H MRS studies because it provides excellent quality of localization. STE localization schemes represent a single voxel (volume element) technique since spectral data are acquired from a single volume at a time. It is also possible to acquire MRS data from a number of volume elements simultaneously utilizing chemical shift imaging (CSI) or spectroscopic imaging (SI)[12]. Furthermore, the STE and SI techniques can be combined for improved spatial resolution[13–15]. In this review we concentrate on the STE sequence.

Stimulated echo localization

In a single voxel technique the volume element is defined by the intersection of three slices. This involves the successive excitation of three slices by the application of three selective RF pulses each in the presence of an orthogonal gradient. Therefore, the STE sequence, which utilizes three RF pulses, is a logical choice for volume localization. The STE localization sequence, combined with the water suppression scheme discussed below is shown in Figure 1. The localization sequence consists of three slice selective RF pulses (P1–P3) along with selective, refocusing, and crusher gradients (indicated by arrows in Figure 1 and described below). The RF pulse P1 in the presence of a gradient applied along the z-direction (referred to as the z-gradient) excites a slice normal to the z-axis. The second and third pulses in the presence of x- and y-gradients excite the other two orthogonal slices. At time $T_E/2$ (T_E is the echo time) following the third RF pulse, the transverse magnetization from the ROI is focused giving rise to the stimulated echo. The position of the ROI can be varied by changing the central frequencies of the RF pulses. The dimensions of the ROI can be varied independently along all the three directions by adjusting RF pulse bandwidth and/or the gradient strength. While the STE sequence is conceptually simple to understand, attention should be paid to some practical problems in its implementation. The three RF pulses used in this sequence generate the desired stimulated echo originating from the ROI but also create a number of unwanted coherences which arise from excitation of columns formed by the intersection of two slices (i.e. two-dimensional localization) and slices (one-dimensional localization). For proper localization, it is important to eliminate the contributions of all the unwanted coherences. This can be achieved by phase cycling the RF and receiver according to the scheme proposed by Fauth *et al.*[16] However, for regional shimming which requires single-shot localization, it is essential to eliminate the contributions from all the unwanted coherences in a single acquisition. This is accomplished by dephasing these coherences through the application of gradients called crushers during the $T_E/2$ and T_M periods (Figure 1). Sometimes the refocusing gradients and extended slice-selective gradients can act as crushers. However, the crusher gradients must be applied carefully to avoid the formation of unwanted echoes[9,10].

The STE sequence enjoys many advantages. The flip angle of each RF pulse is not critical for localization so long as it is less than or equal to 90°. This reduces the set-up time. An important consideration in human studies is the amount of RF power exposure. The RF power deposited varies as the square of the flip angle. Since typical flip angles are 90° or less in the STE sequence, the RF power exposure is small. Finally, studies by Jackson *et al.*[17] indicate the excellent localization quality provided by this sequence. A major disadvantage of the STE sequence is that only half the magnetization from the ROI manifests in the form of a stimulated echo while the other half gives rise to other coherences. Despite this disadvantage, the STE sequence is the most widely used single voxel localization technique for *in vivo* proton MRS studies.

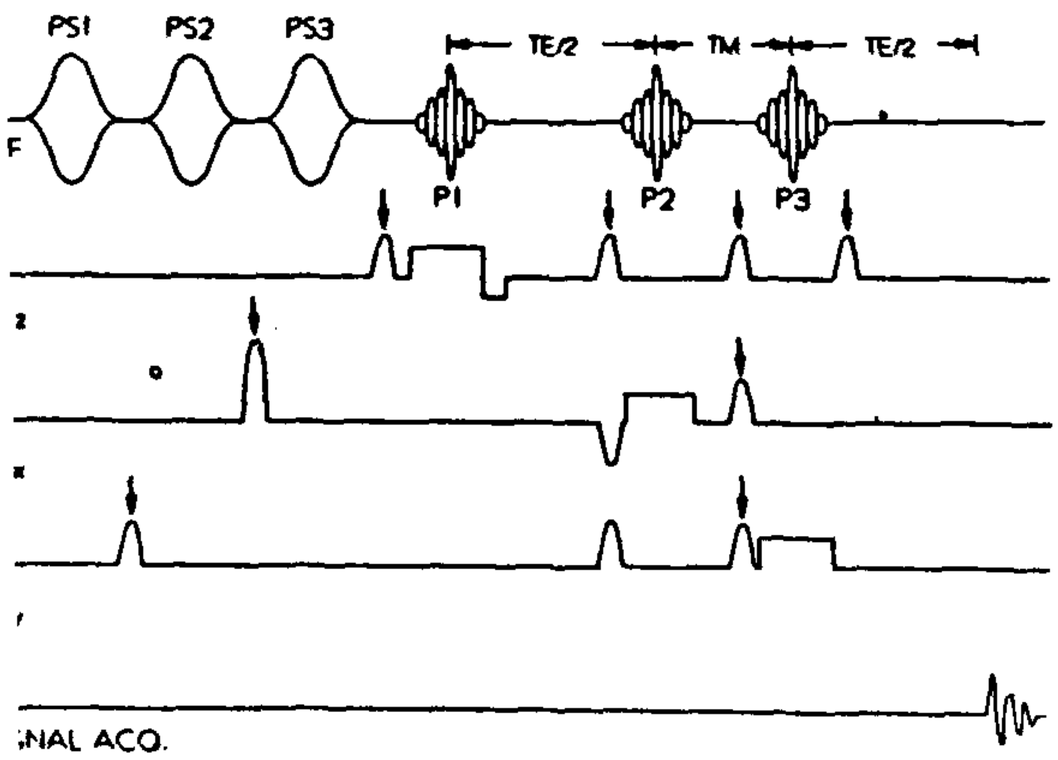

gure 1. The stimulated echo sequence used for water suppressed, calized proton MRS studies. Pulses P1-P3 localize the region of terest (ROI) while water suppression is provided by three emically selective pulses, PS1-PS3. Arrows indicate the crusher adients.

Water suppression

The detection of resonances from biochemicals with low concentrations in the presence of a large water proton signal imposes severe dynamic range demands on the analog-to-digital converter in the MR scanner. It is, therefore, essential to suppress the water resonance for detection and quantification of MR peaks from

biochemicals. Many water-suppression techniques which have been used for *in vivo* MRS were initially developed for high resolution analytical MRS. These techniques, which have been recently reviewed by Hore[18], include pre-saturation, differential relaxation, and selective excitation (or nonexcitation). However, due to short spin–spin relaxation times (T_2) typically encountered in tissues, and because of the intrinsic field inhomogeneities encountered *in vivo*, some of these techniques are not applicable for *in vivo* MRS studies.

The differences in the T_1 and T_2 relaxation times between water and metabolites have been exploited by a number of groups for *in vivo* water suppression[19–23]. However, these techniques provide typical water-suppression factors of around 200. Furthermore, some of these schemes also result in the attenuation of already weak metabolite signals. In the selective excitation for water suppression, narrow bandwidth or 'chemically selective' pulses are applied to the spin system to rotate the water magnetization into the transverse plane while leaving the other spins undisturbed. Because of the relatively short T_2 values encountered *in vivo*, the chemically selective pulse cannot be longer than a few tens of milliseconds which limits the minimum RF bandwidth to 50 to 100 Hz. This technique was used *in vivo*[24,25] for brain MRS studies and typically yields suppression factors of the order of 150–500.

A more efficient and robust water suppression can be achieved by employing multiple saturation pulses as proposed by Doddrell *et al.*[26] who christened the technique SUBMERGE. In this method each saturation pulse is followed by a gradient to dephase the water magnetization in the transverse plane. However, the use of multiple RF pulses and dephasing gradients for water suppression in conjunction with the STE localization sequence can potentially lead to artifacts due to the creation of unwanted echoes. This problem can be eliminated by a proper design of the dephasing gradients following the saturation pulses. Moonen and van Zijl[27] analysed both theoretically and experimentally the performance of this technique for water suppression with minimal creation of unwanted coherences. Their studies indicate that optimal water suppression with minimal artifacts can be obtained using three saturation pulses followed by three dephasing gradients with an amplitude ratio of 1:2:1 or 1:2:4. Similar results were obtained by Jackson and Narayana[28] who performed simulations by numerically solving the Bloch equations. This method can provide water-suppression factors of > 1000. This water suppression scheme, combined with the STE localization sequence (Figure 1), appears to be the most popular technique for single voxel ^{1}H MRS studies.

Even with the excellent water suppression obtained by the SUBMERGE technique, the presence of significant water signal may create problems in the quantification of weak resonances near the water peak. It is possible to eliminate the residual water signal by post-acquisition signal processing as described by Kuroda *et al.*[29] This technique is based on the numerical differentiation of the acquired MR signal. If the carrier frequency is set to the resonant frequency of water protons, the water signal, which varies slowly with time, will be greatly reduced after the numerical differentiation. However, this technique introduces frequency-dependent intensity distortions which must be compensated[30]. Once such a compensation is accomplished the SUBMERGE technique combined with the post-acquisition signal processing is well suited for spectral quantification.

Pulsed gradients

The presence of magnetic field gradients is an indispensable feature of any image-guided localization scheme. These gradients are turned on and off, i.e. pulsed, a number of times for generating localized MRS data. These pulsed gradients create special problems by inducing eddy currents in the conducting metallic structure of the magnet cryostat. The ideal gradient pulse should follow the rectangular current shown in Figure 2,*a*. As shown schematically in Figure 2,*b*, the eddy currents oppose the applied gradients and result in finite gradient rise and settling times (Figure 2,*c*). In a typical magnet without any corrective measures, these settling times could range anywhere from a few tens to about 100 ms. The resulting slowly decaying fields induce phase artifacts which are quite detrimental to localized MRS studies. The gradient settling times can

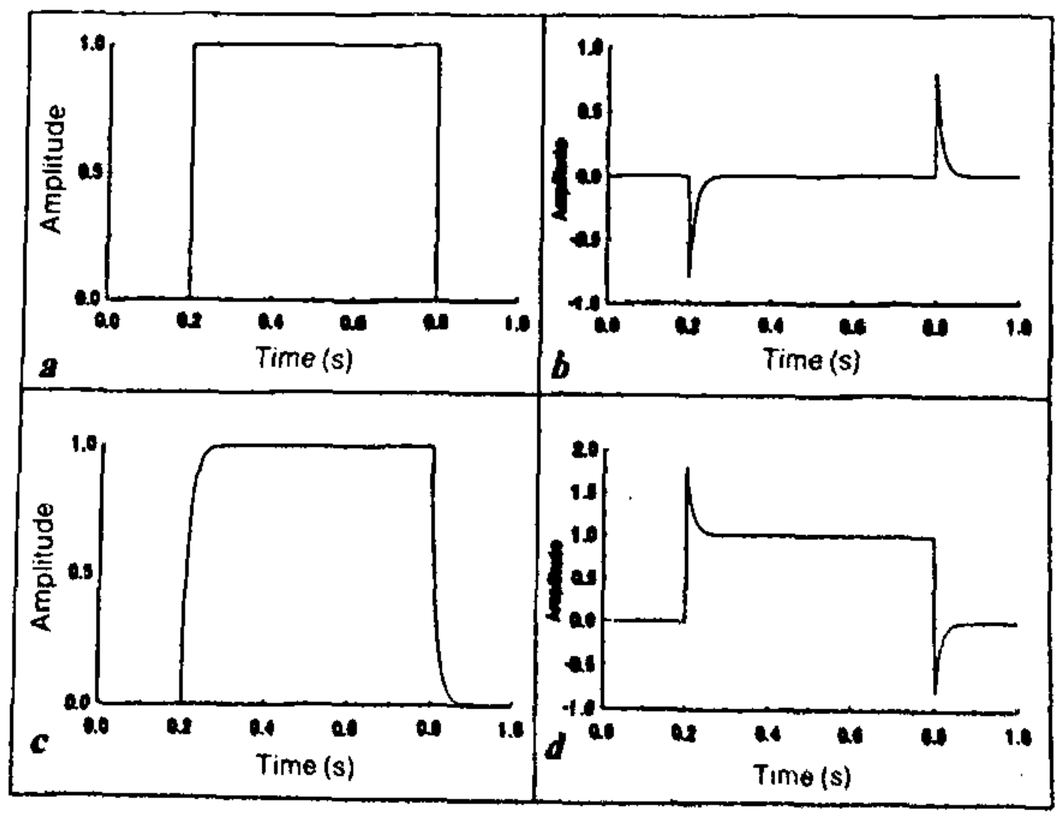

Figure 2. *a–d*, *a*, Ideal gradient field in response to a rectangular current pulse. *b*, Eddy current-generated field opposing the applied gradient. *c*, Actual field produced by the gradient coil with no pre-emphasis. *d*, Input current pulse with pre-emphasis for producing a rectangular gradient pulse.

be minimized by utilizing a compensation or pre-emphasis technique[31] which is briefly described below.

The eddy currents induced in the conducting structure can be modelled as a sum of exponential functions. The opposing magnetic field generated by eddy currents can therefore be compensated by adding a multiexponential current $i(t)$ to the applied rectangular pulse. In practice it is adequate to include three-exponential functions (i.e. three time constants) in the pre-emphasis circuit with independently controllable gains and time constants which are adjusted iteratively and interactively until minimum gradient rise and settling times are observed. The shape of the input current pulse to the gradient coil after compensation is shown in Figure 2,*d*. The technique to measure the gradient rise time was described earlier by Jensen *et al.*[31] and is not repeated here. One of the best techniques to measure the gradient settling times is to monitor the MR spectrum generated using the pulse sequence shown in Figure 3. Following a variable delay, T_g, after the application of a gradient pulse, a short ($\sim 10\,\mu s$) RF pulse is applied. Examination of the MR peak as the value of T_g is successively reduced provides an insight into the gradient settling time. If the gradient field has not settled before the RF pulse is applied, gradient-induced phase shifts will distort the MR lineshape and decrease its amplitude. Thus the minimum delay at which undistorted MR lineshape is observed yields the gradient settling time. With the incorporation of the pre-emphasis technique, it is possible to reduce the gradient rise/settling times to around 1 ms. While the pre-emphasis technique greatly enhances the capability for performing MRS studies, in a few instances this is not adequate, particularly when studies are performed at short echo times. The incorporation of a screened gradient coil system greatly enhances the spectral quality by practically eliminating the coupling of gradient fields with the surrounding metallic structure. The basic idea behind the shielded gradient coil system is to insert an additional gradient coil (called the screen) between the primary coil and the bore tube of the magnet. The screen is driven by an additional current such that the gradient field created by the primary coil is cancelled outside the screened coil, thus eliminating eddy currents induced in the cryostat structure. The shielded gradient coil system can be designed using either the method proposed by Mansfield and Chapman[32,33] or Lowe[34]. In the opinion of the authors and a number of other practising *in vivo* MR spectroscopists, a shielded gradient coil system is an indispensable accessory for image-guided MRS studies. In general, pre-emphasis is combined with the shielded gradient coil for superior performance.

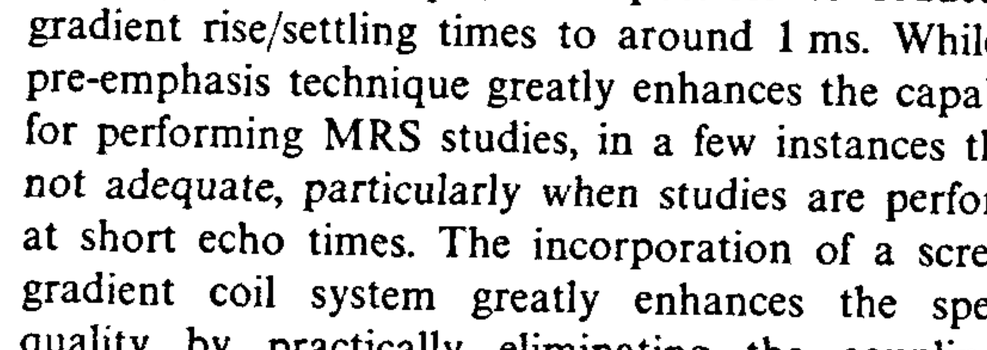

Figure 3. Pulse sequence for determination of the gradient settling time. A short RF pulse ($\sim 10\,\mu s$ duration) is applied at time T_g after the termination of a gradient pulse. The gradient settling time corresponds to the shortest value of T_g at which an undistorted MR lineshape is observed.

In vivo spectroscopy

Experimental

All the MR studies described below were performed on a 1.5 T whole-body scanner (General Electric, Milwaukee) equipped with a shielded gradient coil system. A quadrature bird-cage resonator was used both for RF transmission and signal reception. The global shimming in which all the shim currents are adjusted is performed by the service engineer once every two weeks utilizing a proprietary routine based on chemical shift imaging. A typical patient set-up for brain studies is shown in Figure 4. The sequence of events for MRS studies is briefly described below. Initially multislice MR images in the coronal or axial planes are acquired using a spin echo sequence to locate the ROI. The images are typically T_1-weighted (short T_R, short T_E) with an acquisition time of approximately 1 to 2 min. The ROI is localized using the STE sequence and the magnetic field is homogenized by adjusting the currents in the linear (x, y, z) shims until a water resonance linewidth around 3 to 4 Hz is obtained. This whole operation takes around 10 to 15 minutes. Next the amplitudes of the chemically selective pulses (PS1–PS3 in Figure 1) are adjusted until the water peak is suppressed by a factor of 500 to 2000. This adjustment takes about 5

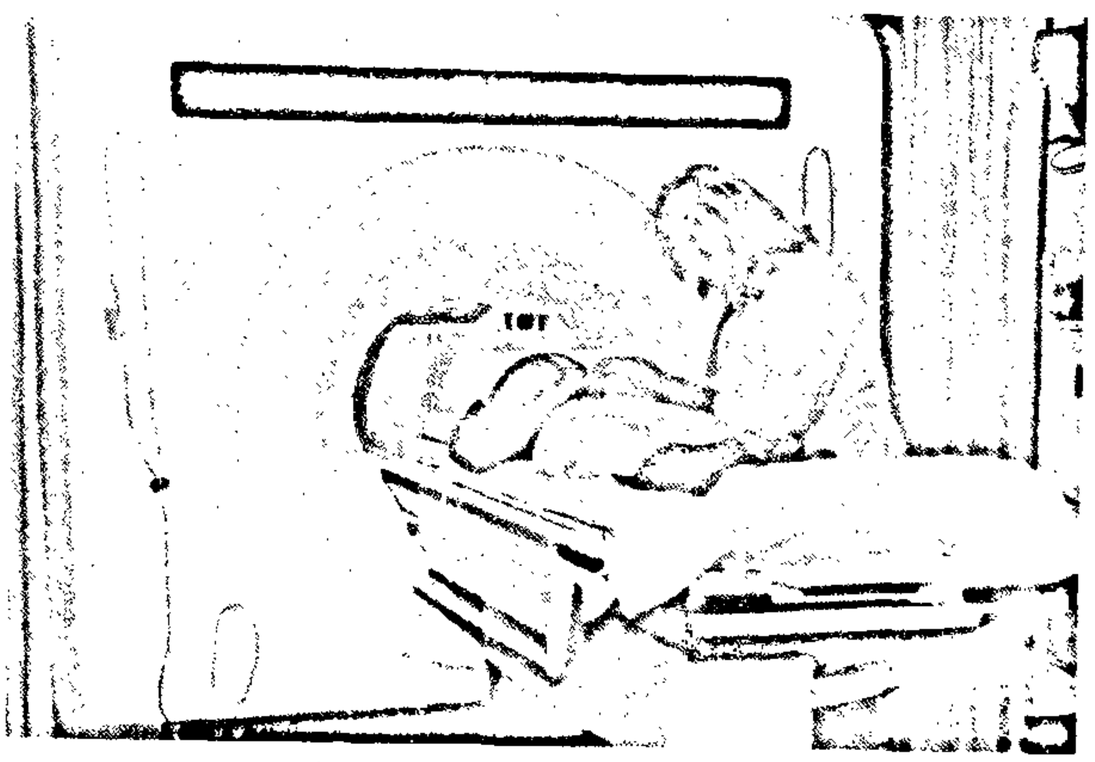

Figure 4. Whole-body magnet with a subject lying in the supine position on the scanner table. The birdcage resonator which surrounds the head can be seen.

min. The actual data acquisition time depends on the size of the ROI and the desired signal-to-noise ratio and may be anywhere between 1 and 30 min. The typical ROI's used in our studies are 8 cc and in this case an acquisition time of 12 min yields adequate signal-to-noise ratio. The whole session for routine MRS lasts less than one hour. The data processing is done off line using a VAX 11/750 computer or a 486-based PC using a combination of commercial and custom software.

Proton spectrum of normal brain

A typical *in vivo* proton spectrum acquired from an 8 cc ($2 \times 2 \times 2$ cm) volume of neural tissue located in the frontal lobe of a normal volunteer is shown in Figure 5. The region from which the spectrum is acquired is indicated by box in the image shown in Figure 6. The image of the ROI is also shown in this figure to demonstrate the localization quality. The spectrum consists of three major resonances from *N*-acetyl aspartate (NAA), creatine + phosphocreatine (Cr + PCr), and phosphotidylcholine (Chol) in addition to a number of minor resonances from glutamate (GLU), glutamine (GLN), γ-aminobutyric acid (GABA), and inositol phosphates (Ins)[35]. The resonances from neurotransmitters such as GLU and GABA and amino acids such as GLN are somewhat broad and are generally difficult to resolve. It is, however, possible to selectively visualize these resonances using spectral editing techniques[36]. It is generally agreed that NAA is found only in neurons even though the precise role of NAA, the most abundant biochemical found in central nervous system tissue, is not known[37,38]. Cr and PCr are important energy substrates while Chol is an important membrane constituent. Thus the proton

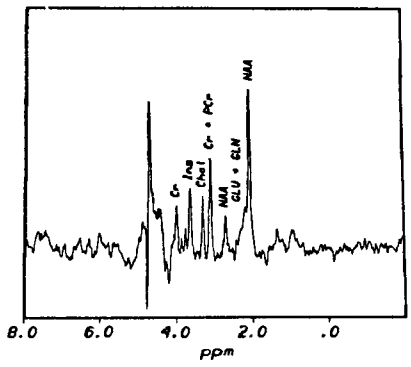

Figure 5. Proton spectrum from a normal brain. The spectrum was acquired from an 8 cc ($2 \times 2 \times 2$ cm) ROI in the frontal lobe. The echo, mixing, and repetition times were $T_E = 20$ ms, $T_M = 7.7$ ms, and $T_R = 3000$ ms respectively. The number of excitations was 256, yielding an acquisition time of approximately 12 min. Various peaks are identified (see text).

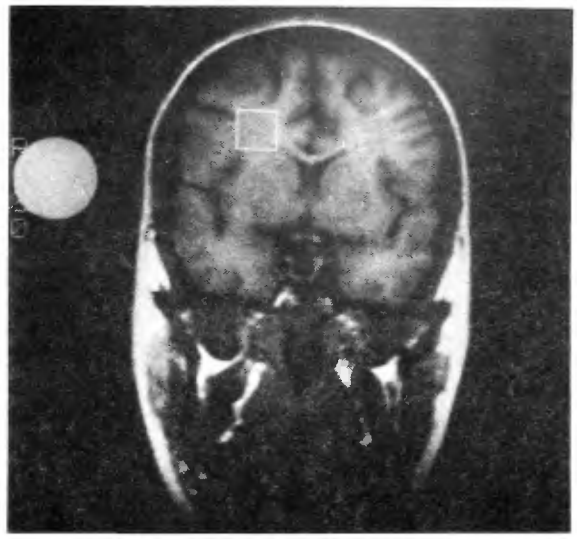

Figure 6. Coronal brain image showing the ROI from which the spectrum shown in Figure 5 was obtained. Acquisition parameters were $T_E = 20$ ms, $T_R = 800$ ms, 5 mm slice thickness, and two excitations. The image of the ROI is also shown to demonstrate localization quality. The standard reference is also shown in this image.

spectrum allows the monitoring of neuronal integrity and brain metabolism. The normal brain spectrum contains very weak lipid signals in spite of high concentration. Cholesterol, phospholipid and galactolipid molecules, which are the major lipid components, are organized in myelin into a highly compact environment that is not conducive to the mobility of constituent hydrogen atoms and therefore are MR invisible. However, in a number of pathologies which include ischaemic injury and multiple sclerosis, the breakdown of membrane releases mobile lipids which are readily seen in the MR spectrum[25,39]. Normal brain has very low concentrations of lactate. Its presence in tissue generally indicates disturbed metabolism. The concentrations of some of these neurochemicals vary with the nature and severity of disease and are reflected in the spectrum.

Determination of the absolute concentrations

The determination of absolute concentrations of molecules with MRS is not straightforward[40]. Therefore, the *in vivo* concentration of neurochemicals is generally expressed relative to an internal standard such as Cr + PCr[24,41]. This assumes that the concentration of the internal reference is unaffected by the disease and this assumption is not generally valid. As pointed out by Bottomley[42], in certain pathologies the absolute concentrations of various biochemicals are

altered relative to normal tissue even though the ratios remain unchanged. It is, therefore, important to determine the absolute concentrations whenever possible. Narayana *et al.*[23] proposed a simple method to determine the absolute concentrations *in vivo* utilizing MRS. A similar technique was independently reported by Roth *et al.*[43] for the determination of phosphate concentrations. The basic idea behind this technique is to incorporate a standard reference of known concentration and relaxation times within the image field-of-view as shown in Figure 6. Following the acquisition of the brain spectrum, the ROI is moved to the centre of the standard sample and a spectrum is acquired under identical conditions. The signal intensity S^x, per unit volume from metabolite x can be expressed as

$$S^x = KN^x \exp\left[-T_E/T_2^x - T_M/T_1^x\right] \left[1-\exp\left(-T_R/T_1^x\right)\right], \quad (1)$$

where N^x is the number of spins per unit volume, K is a parameter which depends on instrumental settings including the receiver gain and RF coil sensitivity, and T_1 and T_2 are the relaxation times. The use of a bird-cage resonator which produces highly homogeneous RF fields[44] assures that the ROI in the brain and the reference sample experience the same RF power. A similar expression can be written for the signal intensity S^s from the reference:

$$S^s = KN^s \exp\left[-T_E/T_2^s - T_M/T_1^s\right] \left[1-\exp\left(-T_R/T_1^s\right)\right]. \quad (2)$$

If N^s, T_1^s, T_2^s, T_1^x and T_2^x are known, it is possible to estimate N^x from equations (1) and (2). Using this technique Narayana *et al.*[23] estimated the absolute concentrations of [NAA] and [Cr + PCr] in gray and white matter of brain. The values along with those determined based on autopsy are shown in Table 1. These results indicate a good agreement between the MRS-determined concentrations and those determined by other standard methods[45].

There are many assumptions implicit in the above method for the estimation of absolute concentrations. It is assumed that these neurochemicals are completely 'MR-visible'. While this appears to be the case for NAA and Cr + PCr, it may not be true for a number of other biochemicals such as glutamate and glutamine.

Table 1. Concentrations of *N*-acetyl aspartate and creatine + phosphocreatine in brain.

Neurochemical (μM/g)	Gray matter	White matter	Ref.
NAA	10.5 ± 2.1^a	5.9 ± 1.7^a	23
	5.73	2.78	37
Cr + PCr	9.2 ± 1.8^a	8.9 ± 1.9^a	23
	8.4	8.4	46

[a]Results are mean ± SD.

Secondly, the number of protons contributing to a given MRS peak should be known. For instance, the absolute concentration of Ins could not be determined because the number of protons contributing to the resonance at 3.6 ppm (from Ins) is not known. Similarly, it is difficult to quantitate lipids found in certain pathologies because the length of the acyl chains, and, therefore, the total number of protons contributing to the lipid peaks, are not known. Another problem that will have significant effect on the estimated concentrations is the overlap of broad resonances with those of the major resonances. The contribution of these minor resonances can be minimized by acquiring the MRS data at long echo times on the order of 50 to 100 ms. At these long echo times, these minor resonances, which are generally broad, would have decayed significantly[46].

In order to monitor the disease with MRS, it is essential to measure the spectral parameters over a period of time. This requires good spectral reproducibility. Quantitative studies by Narayana *et al.*[46] on normal volunteers have shown excellent spectral repeatability over a period of six months and longer. These studies also indicate a significant intersubject variability in the proton MR spectral parameters. These findings suggest the desirability of using the patient as his/her own control whenever possible. In many instances, particularly involving focal disease, the contralateral region of the brain can be used as the control. In those cases where both hemispheres are affected, it becomes necessary to compare the data with age-matched controls. In view of the large intersubject variability such an approach may not be optimal.

Multiple sclerosis

Multiple sclerosis (MS) is a disease of the central nervous system and involves areas of demyelination referred to as plaques. It is a complex disease with a relapsing and remitting course[47]. The pathogenesis of this disease is still unknown. Magnetic resonance imaging is the most sensitive modality to visualize the MS plaques. These plaques appear bright on T_2-weighted (long T_E, long T_R) and density-weighted (short T_E, long T_R) MR images. Often the extent of disease seen on MRI is more dramatic than what the clinical symptoms indicate[48]. This suggests that not all the plaques seen on MRI either contribute directly to clinical symptoms or are active. The ability to distinguish active plaques from inactive ones should greatly help in understanding the pathophysiology of the disease and in management of the patient. Studies by Wolinsky *et al.*[25] show that *in vivo* proton MRS has the potential to differentiate active plaques from inactive ones.

The breakdown of myelin in MS is typically associated with the appearance of lipid droplets within

macrophages[49]. These lipid droplets intensely stain with a variety of histochemical techniques which are dependent, in part, on the disruption of compact myelin lamella and associated esterification of cholesterol and lipids[50]. These breakdown products are mobile and should be detectable with proton MRS. Indeed, proton MRS studies by Wolinsky *et al.*[25] demonstrated the presence of lipids in 8 out of 25 plaques investigated in 17 MS patients. A typical proton spectrum on the high field side of water resonance and the density-weighted image indicating its spatial origin are shown in Figures 7 and 8 respectively. The relatively broad lipid peak around 1 ppm can be clearly seen in the spectrum from

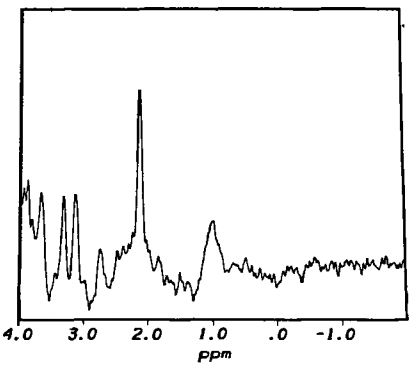

Figure 7. Proton spectrum on the high field side of the water resonance from an ROI containing as MS plaque. In addition to the peaks seen in the normal brain (Figure 5), there is a significant peak at around 1.0 ppm which is due to mobile lipids. The acquisition parameters were the same as described in Figure 5.

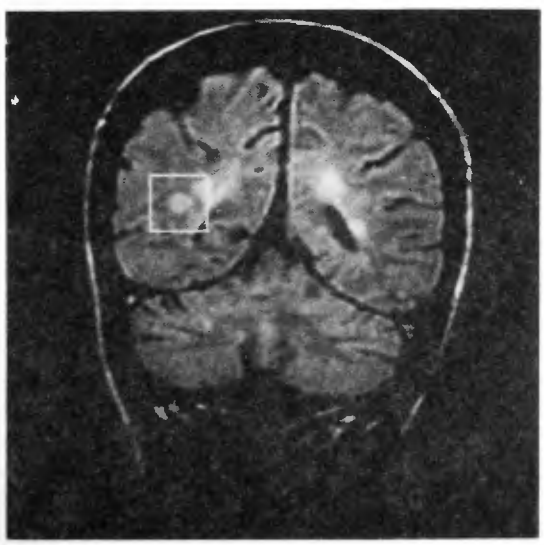

Figure 8. Coronal image showing the ROI from which the spectrum in Figure 7 was obtained. Acquisition parameters were $T_E = 20$ ms and $T_R = 2000$ ms.

the plaque and appears to be an *in vivo* correlate of the early histopathologic changes[49,50].

An important pathologic feature of an active MS plaque is the presence of perivenous inflammatory changes which are usually associated with the local blood-brain-barrier (BBB) breakdown (vascular events)[51,52]. The integrity of the BBB can be probed by performing MRI after the intravenous administration of the paramagnetic contrast agent gadolinium diethylenetriaminepentaacetic acid (GdDTPA). Due to its size, this contrast agent cannot cross the normal BBB. However, GdDTPA can enter the brain if the integrity of the BBB is compromised and alters the T_1 value of tissue water. This altered relaxation time is reflected as a region of enhanced intensity on a T_1-weighted MR image. Several groups observed the presence of a plaque through contrast enhancement even before it became clinically symptomatic or could be detected on unenhanced MRI[53,54].

Thus GdDTPA-enhanced MRI and proton MRS of MS plaques appear to reflect two aspects of the evolution of MS plaques. Enhanced MRI is sensitive to vascular events while proton MRS detects active myelin breakdown. In order to examine if these two events are correlated in the evolution of MS plaques, Narayana *et al.*[55] performed MRS studies on GdDTPA-enhanced plaques in 14 MS patients with recent onset of new clinical symptoms. Of the 31 plaques studied, enhancement was observed in 11 of these plaques in 7 patients. Pre- and post-contrast T_1-weighted images shown in Figure 9 indicate dramatic increase in intensity within 10 min following the administration of GdDTPA. It should be noted that on a T_1-weighted image, unenhanced plaques are not seen clearly. The proton spectrum from this plaque (the ROI indicated by the box) is shown in Figure 10 and is consistent with the presence of lipids in the 0–2 ppm region. Lipid peaks were observed only from 5 of the 11 enhanced plaques. In addition, lipid peaks were observed in 3 out of 20 unenhanced plaques. These studies indicate that demyelination is more frequently associated with active inflammation (as indicated by contrast enhancement) and suggest a causal, but not absolute, relationship between these two processes. As pointed out by Paty[47], 'it is possible that demyelination in MS occurs after multiple episodes of inflammation have repeatedly damaged a particular area of white matter'. It remains uncertain whether active inflammation is an obligatory precursor for myelin breakdown. Longitudinal studies which combine GdDTPA-enhancement and image-guided proton MRS are presently underway and should help clarify this problem.

A qualitative reduction in the [NAA]/[Cr] ratio in some plaques was also observed, perhaps suggesting some neuronal loss[55–57]. Arnold *et al.*[56] and Miller *et al.*[57] have suggested that this reduction in the

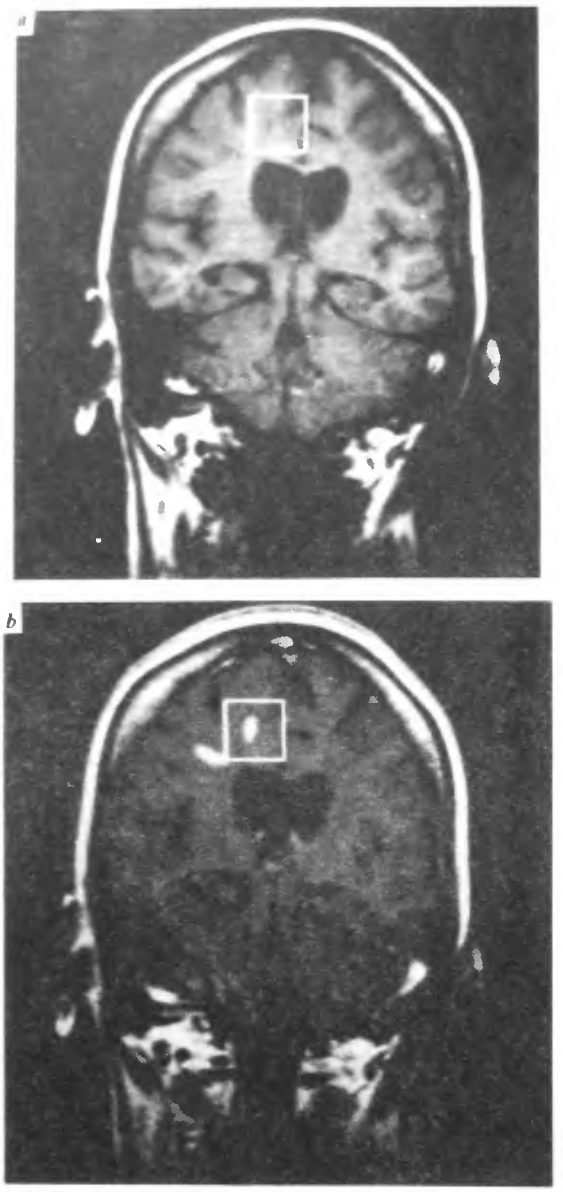

Figure 9. Coronal plane images showing the GdDTPA enhancement of an MS plaque. (*a*) Pre-contrast T_1-weighted image and (*b*) T_1-weighted image acquired five min following administration of GdDTPA. Acquisition parameters were $T_E = 20$ ms and $T_R = 800$ ms.

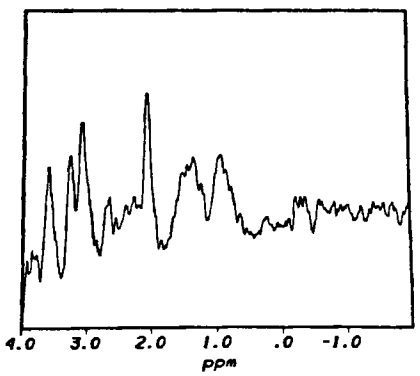

Figure 10. Proton spectrum from the 8-cc ROI containing the enhanced plaque (Figure 9). Note the significant lipid signals in the 0–2 ppm region. Acquisition parameters were the same as described in Figure 5.

[NAA]/[Cr] ratio may be a characteristic feature of chronic plaques. If confirmed, quantitation of the reduction in the NAA amplitude could potentially be another useful index for characterizing MR-defined lesions.

Ischaemic brain injury

The pathophysiological changes associated with ischaemic brain injury include accumulation of lactate due to anaerobic metabolism, depletion of neurochemicals in the first few hours, a return to the normal in the subacute period and the appearance of lipids in the chronic period. Much of the knowledge of these pathophysiological changes is based on animal studies[58,59]. In spite of the significant strides made in understanding the pathophysiological changes associated with cerebral ischaemia, very little is known about the functional recovery from stroke[60,61]. The ability to probe the neuronal integrity (through NAA) and monitor altered lipid and lactate levels with MRS provides an unprecedented opportunity to probe in humans the serial pathological changes following ischaemic brain injury. Such information will be invaluable in gaining an understanding of the cellular events involved in injury repair. In addition, it will be possible to identify any potential specific MRS marker in order to objectively monitor the therapeutic response and to design treatment on an individual basis.

Proton MRS of stroke in humans were initially reported by Barkelback van der Sprenkel *et al.*[62] and Bruhn *et al.*[63] Both these studies dealt with a single patient at one or two time points. The first serial proton MRS studies in humans with documented evidence of ischaemic stroke were reported by Fenstermacher and Narayana[39]. These studies were performed on 4 patients for periods ranging from 3 days to 10 weeks following ictus. The clinical data on these patients are summarized in Table 2. A T_2-weighted coronal MR image acquired 3 days after the ictus in one patient (patient 4) with left cerebellar infarct is shown in Figure 11. The region of infarct can be clearly seen as an area of hyperintensity in the image. The proton spectrum from the infarcted region (indicated by the rectangular box) and the contralateral region from the same patient are shown in Figures. 12, *a* and *b*

Table 2. Summary of patient data for stroke studies.

Subject	Sex/age	Risk factor	Location of injury
1	F/67	PVD	Left visual cortex
2	M/49	CAD/Complications due to angiography	Right perisylvian
3	M/61	PVD	Left cerebellum
4	M/55	DM, HTN, smoking	Left cerebellum

PVD: peripheral vascular disease; CAD: coronary artery disease; DM: diabetes mellitus; HTN: hypertension.

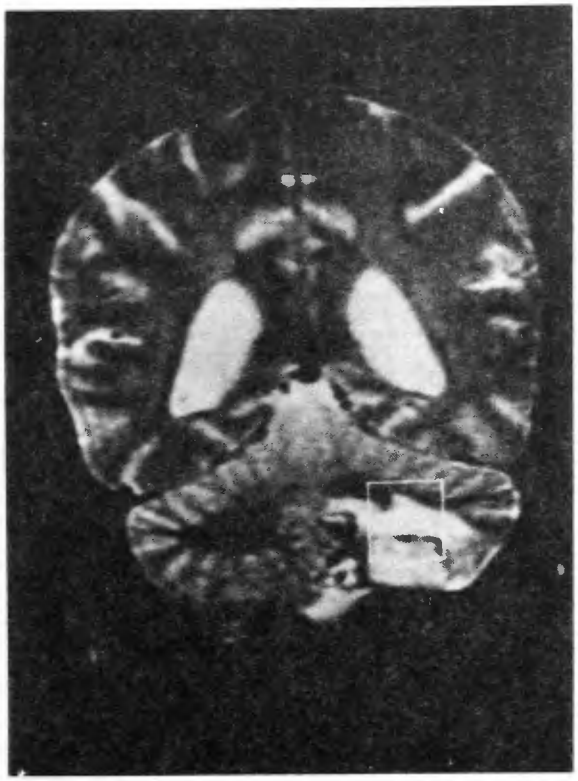

Figure 11. Coronal plane T_2-weighted image ($T_E = 80$ ms, $T_R = 2000$ ms) from a 55-year-old male with left cerebellar infarct. The infarct is seen as an area of hyperintensity. The small hypointense areas seen within this infarct represent petechial haemorrhage.

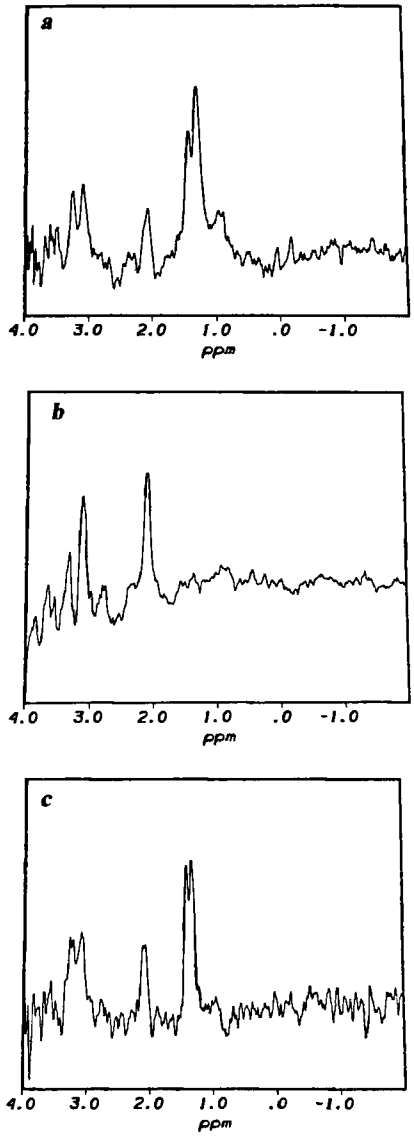

Figure 12. Proton spectrum from an 8-cc ROI in (*a*) the infarct region shown in Figure 11, and (*b*) the normal contralateral region. Acquisition parameters were $T_E = 30$ ms, $T_M = 50$ ms, $T_R = 3000$ ms, and 256 acquisitions. The peaks around 1.5 ppm represent lipids + lactate. (*c*) Spectrum acquired with $T_E = 270$ ms (other parameters unchanged) from the infarct region to demonstrate the presence of lactate. The doublet at 1.3 is due only to lactate.

respectively. The relatively poor resolution observed in the spectrum from the infarcted region is due to the presence of iron as reflected by the petechial haemorrhage seen as areas of hypointensity within the infarct in Figure 11. The spectrum from the infarcted area shows the presence of a peak around 1.5 ppm. This peak has contributions both from lactate and lipids as verified by acquiring the spectrum at a long echo time of 270 ms (Figure 12,*c*). At these long echo times, lipids with short T_2 would have decayed completely while lactate signal still persists. In addition to the appearance of lipids and lactate, the intensities of NAA and Cr + PCr peaks are observed to be only 33% and 44% respectively of the unaffected contralateral region. The Chol peak, however, appears to have retained approximately 90% intensity in the infarcted region. The spectrum from the infarcted region acquired 20 days after ictus shows that the NAA peak has recovered to 57% of the contralateral region, indicating some

neuronal recovery. In addition, lactate has almost completely disappeared as verified by the spectrum acquired at long echo times. The MRS results observed on four patients are summarized in Table 3. A better visual appreciation of this data can be gained by plotting the values of NAA, Cr + PCr, and Chol relative to the contralateral regions pooled from the 4 patients (Figure 13). The partial loss and gradual return of NAA and Cr + PCr to normal can be seen from this plot. The absence of significant change in Chol is quite striking. This probably implies the survival of membranes associated with Chol, i.e. cholinergic neurons. The concomitant decrease in NAA and Cr + PCr with little change in Chol appears to be a marker specific to ischaemic brain injury. The ability to follow sequential metabolic changes *in vivo* in humans as demonstrated by these studies opens up unprecedented opportunities in understanding the pathophysiological changes and instituting new and effective treatments. In order to firmly establish the role of MRS in the clinical management of stroke patients, it is necessary to obtain more serial data beginning earlier and separated by shorter intervals.

The excitatory amino acid neurotransmitter, glutamate, is implicated in ischaemic injury[64–66]. The glutamate peak is generally not well resolved in the proton spectrum. However, use of editing[36] and sophisticated two-dimensional techniques[67] will allow us to visualize the glutamate peak and critically assess the role of this excitotoxin in ischaemic injury. Such studies will open up new avenues in stroke research.

Future directions

Advances in both magnet technology and development of robust image-guided localization techniques in the last four years have moved MRS much closer to the clinical arena. However, the spatial resolution needs to be improved. A combination of single voxel techniques and spectroscopic imaging will help in achieving this objective. This will also help in displayin distribution of various chemicals in the form of i Presently such chemical images are displayed coarse resolution[68]. So far the main emphasis ha placed on major resonances such as NAA, Cr and Chol which are well resolved. With the de ment of spectral editing and two-dimensional niques[67], it will be possible to selectively important neurotransmitters like glutamate and and critically assess their role in various neuro logies. The day may not be too far away physicians and MR spectroscopists sit side by the console to interpret the patient studies.

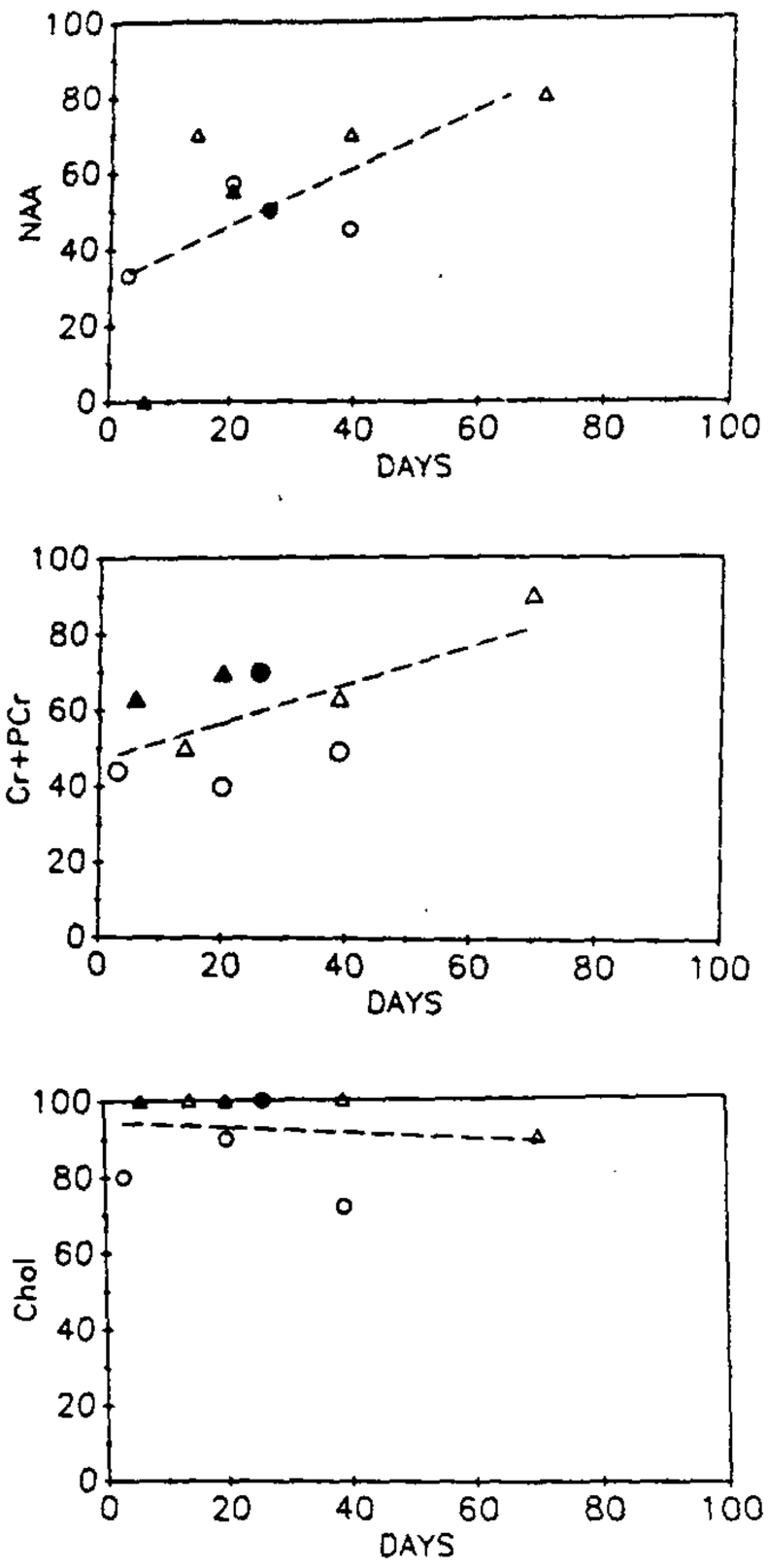

Figure 13. Variation in the levels of NAA, Cr + PCr, and Ch infarct relative to the contralateral region in four patients ov A value of 100 on the ordinate represents the normal level. △ 1, ● Patient 2, ▲ Patient 3, and ○ Patient 4.

Table 3. Percentage peak areas of major resonances in the infarcted region relative to the contralateral control.

Subject	Age of stroke (d)	NAA	Cr + PCr	Chol	Other peaks
1	6	0	63	120	Lipid and lactate
	20	55	70	100	None
2	24	50	70	100	Lipid
	26	50	70	100	None
3	14	70	50	100	Lipid
	39	70	63	100	None
	69	80	>90	>90	None
4	3	33	44	90	Lipid and lactate
	20	57	40	>90	Predominantly lipid
	39	45	49	>90	None

NAA: *N*-acetyl aspartate; Cr + PCr: creatine + phosphocreatine; Chol: choline.

1. Griffiths, R. D. and Edwards, R. H. T., *Biomedical M Resonance Imaging: Principles, Methodology, and App* (eds. Wehrli, F. W., Shaw, D. and Kneeland, J. B. Publishers Inc., New York, 1988, pp. 521–551.
2. Bottomley, P. A., *Radiology*, 1989, **170**, 1.

3. Aisen, A. M. and Chenevert, T. L., *Radiology*, 1989, **173**, 593.
4. Cady, E. B., *Clinical Magnetic Resonance Spectroscopy*, Plenum Press, New York, 1990, pp. 83–139.
5. Demaerel, P. *et al.*, *J. Comp. Asst. Tomog.*, 1991, **15**, 67.
6. Aue, W. P., *Rev. Magn. Reson. Med.*, 1986, **1**, 21.
7. Narayana, P. A. and Delayre, J. L., *Magnetic Resonance Imaging*, Second Edition, (eds. Partain, C. L.), W. B. Saunders Co., Philadelphia, USA 1988, pp. 1609–1630.
8. Frahm, J., Merboldt, K. -D., Hanicke, W. and Haase, A., *J. Magn. Reson.*, 1985, **64**, 81.
9. Granot, J., *J. Magn. Reson.*, 1986, **70**, 488.
10. Kimmich, R. and Hoepfel, D., *J. Magn. Reson.*, 1987, **72**, 379.
11. Frahm, J., Merboldt, K.-D. and Hanicke, W., *J. Magn. Reson.*, 1987, **72**, 502.
12. Brown, T. R., Kincaid, B. M. and Ugurbil, K., *Proc. Natl. Acad. Sci. USA*, 1982, **79**, 3523.
13. Segebarth, C. M., Baleriaux, D. F., Luyten, P. R. and den Hollander, J. A., *Magn. Reson. Med.*, 1990, **13**, 62.
14. Flamig, D., *Book of Abstracts*, 7th Annual Meeting, Society of Magnetic Resonance in Medicine, Berkeley, CA, 1988, pp. 927.
15. Jackson, E. F., Narayana, P. A. and Flamig, D. P., *Magn. Reson. Imag.*, 1990, **8**, 153.
16. Fauth, J.-M., Schweiger, A., Braunschweiler, L., Forrer, J. and Ernst, R. R., *J. Magn. Reson.*, 1986, **66**, 74.
17. Jackson, E. F., Narayana, P. A. and Kudrle, W. A., *J. Magn. Reson.*, 1988, **80**, 23.
18. Hore, P. J., *Methods Enzymol.*, 1989, **176**, 64.
19. Bottomley, P. A., Edelstein, W. A., Foster, T. H. and Adams, W. A., *Proc. Natl. Acad. Sci. USA*, 1985, **82**, 2148.
20. Keller, P. J. *et al.*, *Book of Abstracts*, 5th Annual Meeting, Society of Magnetic Resonance in Medicine, Berkeley, CA, 1986, pp. 983.
21. Narayana, P. A., Hazle, J. D., Jackson, E. F., Fotedar, L. K. and Kulkarni, M. V., *Magn. Reson. Imag.*, 1988, **6**, 481.
22. Narayana, P. A. *et al.*, *Magn. Reson. Med.*, 1988, **8**, 151.
23. Narayana, P. A. *et al.*, *J. Magn. Reson.*, 1989, **83**, 44.
24. Frahm, J. *et al.*, *Magn. Reson. Med.*, 1989, **11**, 47.
25. Wolinsky, J. S., Narayana, P. A. and Fenstermacher, M. J., *Neurology*, 1990, **40**, 1764.
26. Doddrell, D. M. *et al.*, *J. Magn. Reson.*, 1986, **70**, 176.
27. Moonen, C. T. W. and van Zijl, P. C. M., *J. Magn. Reson.*, 1990, **88**, 28.
28. Jackson, E. F. and Narayana, P. A., *Book of Abstracts*, 9th Annual Meeting, Society of Magnetic Resonance in Medicine, Berkeley, CA, 1990, pp. 1072.
29. Kuroda, Y., Wada, A., Yamazaki, T. and Nagayama, K., *J. Magn. Reson.*, 1989, **84**, 604.
30. Jackson, E. F. and Narayana, P. A., *Book of Abstracts*, 9th Annual Meeting, Society of Magnetic Resonance in Medicine, Berkeley, CA, 1990, pp. 1074.
31. Jensen, D. J., Brey, W. W., Delayre, J. L. and Narayana, P. A., *Med. Phys.*, 1987, **14**, 859.
32. Mansfield, P. and Chapman, B., *J. Magn. Reson.*, 1986, **66**, 573.
33. Mansfield, P. and Chapman, B., *J. Magn. Reson.*, 1987, **72**, 211.
34. Lowe, I. J., 28th Annual Experimental NMR Conference, 1987, Poster No: MF71.
35. Petroff, O. A. C., *Comp. Biochem. Physiol.*, 1988, **90B**, 249.
36. Rothman, D. L., Behar, K. L., Hetherington, H. P. and Shulman, R. G., *Proc. Natl. Acad. Sci. USA*, 1984, **81**, 6330.
37. Nadler, J. V. and Cooper, J. R., *J. Neurochem.*, 1972, **19**, 313.
38. Birken, D. L. and Oldendorf, W. H., *Neurosci. Biobehav. Rev.*, 1989, **13**, 23.
39. Fenstermacher, M. J. and Narayana, P. A., *Invest. Radiol.*, 1990, **25**, 1034.
40. Tofts, P. S. and Wray, S., *NMR Biomed.*, 1988, **1**, 1.
41. Hanstock, C. C., Rothman, D. L., Prichard, J. W., Jue, T. and Shulman, R. G., *Proc. Natl. Acad. Sci. USA*, 1988, **85**, 1821.
42. Bottomley, P. A., Hardy, C. J., Cousins, J. P., Armstrong, M. and Wagle, W. A., *Radiology*, 1990, **176**, 407.
43. Roth, K. *et al.*, *J. Magn. Reson.*, 1989, **81**, 299.
44. Hayes, C. E., Edelstein, W. A., Schenck, J. F., Mueller, O. M. and Eash, M., *J. Magn. Reson.*, 1985, **63**, 622.
45. Lewis, L., Ljunggrent, B., Ratcheson, R. A. and Siesjo, B. K., *J. Neurochem.*, 1974, **23**, 673.
46. Narayana, P. A., Johnston, D. and Flamig, D. P., *Magn. Reson. Imag.*, 1991, **9**, 303.
47. Paty, D. W., *Can. J. Neurol. Sci.*, 1988, **15**, 266.
48. Thompson, A. J. *et al.*, *Br. Med. J.*, 1990, **300**, 631.
49. Prineas, J. W., *Handbook of Clinical Neurology* (eds. Vinken, P. J., Bruyn, G. W. and Klawans, H. L.), No. 47, Demyelinating diseases, Elsevier, Amsterdam, 1985, Vol. 3, pp. 213.
50. Adams, C. W. M., Paston, R. N. and Buk, S. J., *J. Neurol. Sci.*, 1989, **92**, 291.
51. Pozzilli, C. *et al.*, *J. Neurol. Psychiatry*, 1988, **51**, 1058.
52. James, P. B., *Lancet*, 1989, **1**, 46.
53. Grossman, R. I. *et al.*, *Radiology*, 1986, **161**, 721.
54. Kermode, A. G. *et al.*, *Brain*, 1990, **113**, 1477.
55. Narayana, P. A., Wolinsky, J. S., Jackson, E. F. and McCarthy, M., *Neurology*, 1991 (submitted).
56. Arnold, D. L., Matthews, P. M. and Antel, J., *Magn. Reson. Med.*, 1990, **14**, 154.
57. Miller, D. H. *et al.*, *Lancet*, 1991, **337**, 58.
58. Brant-Zawadzki, M., Weinstein, P., Bartkowski, H. and Mosely, M., *Am. J. Neuroradiol.*, 1987, **8**, 39.
59. Chang, L. H., Shirane, R., Weinstein, P. R. and James, T. L., *Magn. Reson. Med.*, 1990, **13**, 6.
60. Heiss, W.-D. *et al.*, *Cerebrovascular Diseases* (eds. Ginsberg, M. D. and Dietrich, W. D.), Raven Press, New York, 1989, pp. 345.
61. Powers, W. J. and Fox, P. T., *Cerebrovascular Diseases* (eds. Ginsberg, M. D. and Dietrich, W. D.), Raven Press, New York, 1989, pp. 353.
62. van der Sprenkel, B. J. W., Luyten, P. R., van Rijen, P. C., Tulleken, C. A. F. and den Hollander, J. A., *Stroke*, 1988, **19**, 1556.
63. Bruhn, H. *et al.*, *Magn. Reson. Med.*, 1989, **9**, 126.
64. Auer, R. N. and Siesjo, B. K., *Ann. Neurol.*, 1988, **24**, 699.
65. Albers, G. W., Goldberg, M. P. and Choi, D. W., *Ann. Neurol.*, 1989, **25**, 398.
66. Benveniste, H. *et al.*, *J. Cereb. Blood Flow Metab.*, 1989, **9**, 629.
67. Prestegard, J. H., *Pulse Methods in 1D and 2D Liquid-Phase in MR* (ed. Brey, W. S.), Academic Press, New York, 1988, pp. 435.
68. Luyten, P. R. *et al.*, *Radiology*, 1990, **176**, 791.

ACKNOWLEDGEMENTS. The work described in this article is a result of collaborations with a number of investigators. In particular we would like to thank Ian J. Butler, Marc A. Fenstermacher, John M. Slopis, and Jerry S. Wolinsky. This work was supported by NIH (1 RO1 CA42280-01 and 1 RO1 GM38272-01), the Muscular Dystrophy Association, the National Multiple Sclerosis Society, and the John S. Dunn Foundation.